

Elastic interactions of active cells with soft materialsI. B. Bischofs,¹ S. A. Safran,² and U. S. Schwarz^{1,3,*}¹Max Planck Institute of Colloids and Interfaces, 14424 Potsdam, Germany²Department of Materials and Interfaces, Weizmann Institute of Science, Rehovot 76100, Israel³Institute of Theoretical Physics, University of Leipzig, 04103 Leipzig, Germany

(Received 12 September 2003; published 27 February 2004)

Anchorage-dependent cells collect information on the mechanical properties of the environment through their contractile machineries and use this information to position and orient themselves. Since the probing process is anisotropic, cellular force patterns during active mechanosensing can be modeled as anisotropic force contraction dipoles. Their buildup depends on the mechanical properties of the environment, including elastic rigidity and prestrain. In a finite sized sample, it also depends on sample geometry and boundary conditions through image strain fields. We discuss the interactions of active cells with an elastic environment and compare it to the case of physical force dipoles. Despite marked differences, both cases can be described in the same theoretical framework. We exactly solve the elastic equations for anisotropic force contraction dipoles in different geometries (full space, half space, and sphere) and with different boundary conditions. These results are then used to predict optimal position and orientation of mechanosensing cells in soft material.

DOI: 10.1103/PhysRevE.69.021911

PACS number(s): 87.17.Aa, 87.18.Hf, 61.72.Ji

I. INTRODUCTION

Anchorage-dependent cells like fibroblasts in connective tissue show a remarkable degree of mechanical activity. The first quantitative measurements of cellular traction were performed with the elastic substrate method in the early 1980s by Harris and co-workers, who found that cells exert much larger forces than previously thought [1,2]. During recent years, the elastic substrate method has been improved considerably [3,4]. In particular, a new variant involving micropatterning has been developed, which allows one to resolve individual forces exerted at single focal adhesions [5,6]. *Focal adhesions* are mature adhesion contacts based on transmembrane proteins from the integrin family. Since they connect the extracellular matrix and the actin cytoskeleton, they can transmit internal forces to the environment and external forces to the cell. Using micropatterned elastic substrates, it was found that fibroblasts typically exert forces of 10 nN at mature focal adhesions [5,6]. Using a bed of flexible micro-needles, similar values were found for smooth muscle cells [7]. Since adherent cells can have up to hundreds of focal adhesions, the overall force exerted by the cell can amount to microNewton. The forces exerted by cells on their environment result from nonequilibrium processes inside the cell and are generated by myosin II molecular motors interacting with the actin cytoskeleton. Since typical forces produced by molecular motors are in the picoNewton range [8], there must be up to 10^6 myosin II molecular motors contributing to overall cell traction.

When Harris and co-workers first discovered these large forces, they concluded that they are required for the physiological function of the specific cell type under consideration. For example, fibroblasts are believed to maintain the integrity of connective tissue by mechanically pulling on the

collagen fibers. Moreover, they are an integral part of the wound contraction process. Harris and co-workers also noticed that cells react to mechanical changes in their environment caused by traction of other cells. Since cells are known to align along topographic features in their environment (*contact guidance*), they suggested that cells react to traction-induced reorganization of collagen fibers. This mechanism amounts to a mechanical interaction of cells and has been addressed theoretically in coupled transport equations for fiber and cell degrees of freedom [9,10].

During recent years, the sophisticated use of elastic substrates has shown that cells also react to purely elastic features in their environment, including rigidity, rigidity gradients and prestrain [11–13]. It is now generally accepted that these effects are related to the special properties of focal adhesions [14]. In particular, it has been shown that application of external force leads to growth of focal adhesions and therefore to strong signaling activity [15–17]. The same aggregation has been found for mature focal adhesions under internally generated force [5–7], suggesting that focal adhesions act as mechanosensors that convert force into biochemistry and vice versa. Therefore the mechanical activity of cells is not only related to the physiological function of their cell type, but is also a general way to collect information about the mechanical properties of the environment (*active mechanosensing*). There is strong evidence that this mechanism is involved in many important physiological situations, including tissue maintenance, wound healing, angiogenesis, development, and metastasis [18–20].

The dynamics of focal adhesions is a subject of much current research [21]. Anchorage-dependent cells constantly assemble and disassemble focal adhesions, thereby probing the mechanical properties of their environment. Initial focal adhesions (*focal complexes*) are local processes based on integrin clustering. If initial clustering is stabilized by the properties of the extracellular environment, focal complexes can mature into focal adhesions. In this case, they connect to the actin cytoskeleton and a contractile force pattern builds

*Corresponding author. Email address: Ulrich.Schwarz@mpikg-golm.mpg.de

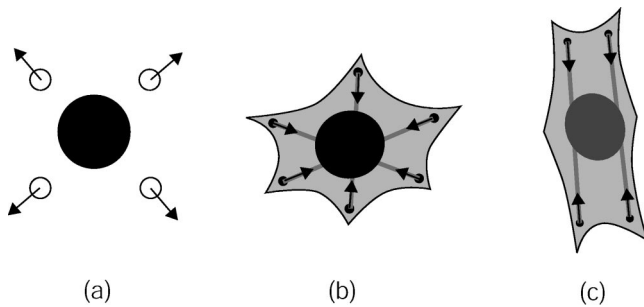


FIG. 1. Schematic representation of physical and cellular force dipoles. (a) Physical case: an intercalated defect deforms the simple cubic host lattice, thus acting as an isotropic force expansion dipole. (b) Cellular case: anchorage-dependent cells probe the mechanical properties of the soft environment through their contractile machinery. Actin stress fibers (lines) are contracted by myosin II molecular motors and are connected to the environment through focal adhesions (dots). Even if cell morphology is round or stellate, different stress fibers probe different directions of space and compete with each other for stabilization of the corresponding focal adhesions. Therefore the probing process can be modeled as anisotropic force contraction dipole. (c) Cell morphology becomes elongated in response to anisotropic external stimuli, during locomotion or spontaneously during times of strong mechanical activity. Then most stress fibers run in parallel and the whole cell appears as an anisotropic force contraction dipole.

up, which is actively generated by myosin II molecular motors interacting with the actin cytoskeleton. The minimal configuration of this machinery is a set of two focal adhesions connected by one bundle of actin filaments (*stress fiber*), which leads to a pinchlike force pattern. In condensed matter physics, such an object is known as an *anisotropic force contraction dipole* [22]. The concept of force dipoles has been applied before mainly for the description of point defects in traditional condensed matter systems, including hydrogen in metal (e.g., platinum) [23], atoms adsorbed onto crystal faces (e.g., argon on gold) [24], or intercalation compounds (e.g., lithium in graphite) [25]. The concept of force dipoles has also been used to model active biological particles in a fluid environment, e.g., ion pumps [26] and rotary motors [27] embedded in fluid membranes, or self-propelled particles like swimming bacteria [28]. Recently, we have suggested to use the concept of force dipoles to model the mechanical activity of cells [29]. Cells in an isotropic environment often show isotropic (that is round or stellate) morphologies. However, since the focal adhesion dynamics is local, even in this case there is an anisotropic probing process, that can be modeled by anisotropic force contraction dipoles. As we will argue below, only an anisotropic probing process can react to anisotropies in the environment. The anisotropy of focal adhesion dynamics becomes apparent when stress fibers start to orient in one preferential direction, either spontaneously during a period of large mechanical activity, or as a response to some external anisotropy, or during cell locomotion. In this case, cellular dipoles have been measured to be of the order of $P \approx -10^{-11} \text{J}$ (this corresponds to two forces of 200 nN each, separated by a distance of 60 μm) [6,30]. In Fig. 1 we show schematic representations

of the physical and cellular cases discussed here.

In order to sense the mechanical properties of their environment, cells can make use of the fact that these properties modulate the build up of their own force patterns. In this paper, we focus on the role of stress and strain in the extracellular material for cellular decision making in regard to positioning and orienting in a soft environment. In order to calculate how stress and strain are propagated in the environment, the extracellular material is modeled using isotropic linear elasticity. This is certainly true for synthetic elastic substrates (usually made from polydimethylsiloxane or polyacrylamide). The typical physiological environment for anchorage-dependent cells are hydrogels, whose mechanical properties are more difficult to model, in particular due to their viscoelastic and nonlinear behavior. Yet our calculations will show that our model has large predictive power also for this case, possibly because elastic deformations of hydrogels become encoded in plastic changes that later can be detected by active mechanosensing in a similar way as persistent elastic deformations. Given the assumption of isotropic linear elasticity, we can calculate how stress and strain follows from the force dipoles by solving the elastic equations for the geometry and boundary conditions of interest.

The most critical part of our modeling is the way in which physical or cellular force dipoles react to stress and strain in their environment. This subject has been treated extensively for the case of atomic defects in traditional condensed matter systems [23–25]. Here defects are usually modeled as isotropic force expansion dipoles. The equilibrium configuration follows by minimizing the sum of the elastic energy of the strained medium and the direct interaction energy between force dipole and elastic environment. The first term represents a restoring force and raises the energy (i.e., its sign is always positive), while the second term is a driving force that reduces the total energy (i.e., its contribution will always be negative). The equilibrium configuration will correspond to the minimum of the total energy as a function of position and orientation of the force dipoles, which results in an effective, so-called *elastic interaction* between the force dipole and other dipoles, sample boundaries or external strain fields. One central result of these studies is that the direct interaction between isotropic force dipoles in an isotropic elastic material vanishes [22] and that they interact through a boundary-induced (*image*) interaction that varies on the length scale of the sample size (leading to *macroscopic modes*) [23]. For anisotropic force dipoles, the direct elastic interaction does not vanish. Recently, we have predicted that the competition between direct and image interactions should lead to hierarchical structure formation, with the direct interaction leading to structure formation on a length scale set by the elastic constants and similar to that of electric quadrupoles [29]. We suggested that such a behavior should be expected for artificial or inert cells, that is, for physical particles with a static force contraction dipole, but without any internal dynamic or regulatory response.

In contrast to this physical case, the effective behavior of active cells usually follows from dynamic and tightly regulated nonequilibrium processes inside the cell. More recently, we have shown that despite this severe complication, it is

still possible to describe the active response of mechanosensing cells in an elastic material in the same framework as the physical case [31]. In detail, motivated mainly by recent experiments with elastic substrates [11–13], we have suggested that effective cellular behavior can be described as simple preference for large effective stiffness in the environment (including both rigidity and tensile prestrain). Moreover, we have shown that this principle is equivalent to minimization of the energy which the cells have to invest into straining the environment in order to build up the force dipole used for probing the mechanical properties of the environment. One likely explanation for the observed active behavior of cells is that the buildup of force at focal adhesions is more efficient in a stiff environment. Since this approach allows us to use the same framework as in the physical case, we were able to derive elastic interaction laws between cells and their elastic environment which are in good agreement with experimental observations for fibroblasts both on elastic substrates and in hydrogels. In particular, the direct elastic interaction between cells has been predicted to be similar to that of electric dipoles, leading to strings of cells [31].

In this paper, we present a unifying formalism for theoretical models for elastic interactions for both physical force dipoles and active cells. In particular, we consider interactions with external strain fields, sample boundaries or other physical force dipoles/cells. Although there are marked conceptual differences between the physical and cellular cases, they both require to solve the elastic boundary value problem to predict the resulting structure formation. Since cells are modeled as anisotropic force dipoles, these calculations are in general more involved than similar calculations for isotropic force dipoles. Moreover, in contrast to earlier calculations for the physical case, we are interested not only in the effect of free, but also of clamped boundaries, which are known to induce mechanical activity of cells [32]. Our paper is divided into two parts. In the first part, we discuss the details of our modeling, in particular, the difference between physical and cellular force dipoles. In the second part, we apply our model to several cases of interest. Here we present exact solutions of the elastic equations for anisotropic force dipoles in full space, half space, and sphere, and apply them both to physical and cellular force dipoles. For example, we show that cells are attracted and repelled by clamped and free sample boundaries, respectively. In the case of physical force dipoles, this behavior is inverted. Our predictions for cells explain many experimental findings reported in the literature, can be used for rational design of tissue equivalents, and show that physical concepts can provide new and important insight into cell biology, provided that they are applied with adequate modifications.

II. MODELING

A. Force multipoles

In the following, we model a mechanically active cell as a localized force distribution in an elastic medium. In order to describe its mechanical action, we use the concept of a force multipolar expansion, which has been applied before for the description of point defects in condensed matter systems

[23–25]. Consider a force distribution localized around the origin. Then the force multipoles are defined as [22]

$$P_{i_1, \dots, i_n} = \int s_{i_1} \cdots s_{i_n} f_i(\vec{s}) d^3s, \quad (1)$$

where f_i is the force density and d^3s denotes a volume integral. The first order term is the vector of overall force P_i and the second order term is the force dipole P_{ij} , a tensor of rank two. For both the cellular and physical situation we are interested in, we can assume local forces. For pointlike defects, one can, moreover, assume that the overall force vanishes, because due to Newton's third law, the forces exerted by the defect on the elastic medium and by the elastic medium on the defect have to balance each other (the same argument applies to point defects in a fluid medium [26–28]). For cells, the situation is more complicated, because they are at the same time in contact with the elastic matrix and an aqueous medium, thus unbalanced forces might appear in the elastic matrix, which are balanced by viscous forces in the aqueous medium. However, viscous processes in the fluid medium decay very rapidly on the time scale of cell movement. Therefore unbalanced forces might occur for short periods of time, e.g., during back retraction of locomoting cell, but during most of the time, cells can be expected to be in mechanical equilibrium, as suggested by experiments measuring force patterns of both stationary and locomoting cells on elastic substrates [4,6]. Our model for cellular force patterns can be interpreted as one stress fiber connecting two focal adhesions. Obviously this minimal system obeys mechanical equilibrium. Then overall force vanishes and the force dipole is the first relevant term in the multipolar expansion Eq. (1).

Force dipoles are classified according to their symmetry properties into isotropic dipoles (centers of contraction or dilation), anisotropic dipoles without moment and anisotropic force dipoles with moment [33]. Force dilatation and force contraction dipoles have only positive and only negative eigenvalues, respectively. For example, in three dimensions three pairs of juxtaposed forces, one for each coordinate direction, form an isotropic force dipole, where $P_{ij} = P \delta_{ij}$. Such a force dipole describes a spherical inclusion in a simple cubic lattice, see Fig. 1(a) [23]. Applied to two dimensions, it describes atomic defects adsorbed onto a substrate [24]. An anisotropic force dipole without moment is a nondiagonal, but symmetric tensor. For example, for a couple of juxtaposed forces with a dipole strength P and an orientation in direction \vec{l} , we can write the force dipole tensor as $P_{ij} = P \hat{l}_i \hat{l}_j$. Such dipoles are used below to describe the probing force patterns of cells, see Figs. 1(b) and 1(c) [29]. An anisotropic force dipole without moment oriented in the z direction reads $P_{ij} = P \delta_{iz} \delta_{jz}$ and describes, for example, an atomic defect intercalated in graphite [25]. Finally, an anisotropic force dipole with an angular moment describes a set of two opposing forces \vec{F} separated by a distance \vec{l} oriented arbitrarily with respect to \vec{F} , which leads to $P_{ij} \neq P_{ji}$. In this paper, we only consider force dipoles without such moments.

B. Interaction between physical dipoles and an elastic medium

The elastic medium surrounding a particle can mediate an *elastic* interaction with other particles, sample boundaries or external strain fields. It is important to note that this effect requires a *direct* interaction of the particle with its elastic environment. In traditional condensed matter systems, the direct interaction is usually a quantum effect (e.g., Born repulsion for defects intercalated into a crystal lattice or van der Waals attraction for defects adsorbed onto a crystal lattice). The interaction of a single particle localized at \vec{r} with the elastic medium can be described by an interaction potential $V_d(\vec{r}, \vec{u})$, which not only depends on position \vec{r} , but which also is a functional of the displacement field $\vec{u}(\vec{r}')$ of the elastic medium. For a fixed particle position \vec{r} , we can expand the interaction potential with respect to the displacement field

$$V_d(\vec{r}, \vec{u}) \approx - \int f_i(\vec{r} + \vec{s}) u_i(\vec{r} + \vec{s}) d^3s, \quad (2)$$

where $f_i = -\delta V_d / \delta u_i|_{u_i=0}$ is the force density exerted by the defect onto the elastic medium in its undeformed reference state. Here and in the following, summation over repeated indices is always implied. The expansion can be terminated after the linear term because we assume small deformations, or, equivalently, small forces. This linearized interaction potential is widely used in the literature on elastic defects in traditional condensed matter materials [23–25]. For later use, we also note that Eq. (2) can be rewritten in terms of the force multipoles defined in Eq. (1), if one makes the assumption that the interaction of the defect with the medium is short ranged. Then

$$V_d(\vec{r}, \vec{u}) \approx - \sum_{n=0}^{\infty} \frac{1}{n!} P_{i_1, \dots, i_n} u_{i_1, \dots, i_n}(\vec{r}), \quad (3)$$

where indices after the comma denote derivatives of the displacement field with respect to position ($u_i = \partial u / \partial r_i$). In this way, all the details of the direct interaction between medium and defect are subsumed in the defect force pattern and one can study elastic effects in different materials within a common theoretical framework, as long as the two assumptions of small and localized forces are valid.

The displacements of the elastic medium are controlled by a competition between the direct interaction between defect and medium and the elastic strain energy of the medium under the constraints of adequate boundary conditions. The strain energy is [34]

$$V_e = \frac{1}{2} \int d^3r C_{ijkl} u_{ij}(\vec{r}) u_{kl}(\vec{r}), \quad (4)$$

where $u_{ij}(\vec{r})$ is the strain tensor and C_{ijkl} the elastic constant tensor of the medium. Consider now the general case of an elastic medium subject to loading with defects with an overall volume force density $\vec{f}(\{\vec{r}^\alpha\}, \vec{r}) = \sum_\alpha \vec{f}^\alpha(\vec{r})$, where α numbers the different defects. Then the total energy of the system is

$$V_t = \frac{1}{2} \int d^3r C_{ijkl} u_{ij}(\vec{r}) u_{kl}(\vec{r}) - \int d^3r f_i(\{\vec{r}^\alpha\}, \vec{r}) u_i(\vec{r}) - \oint dS f_i^s(\vec{r}) u_i(\vec{r}), \quad (5)$$

where the first term is the strain energy V_e and the second term the direct interaction $V_d = \sum_\alpha V_d(\vec{r}^\alpha)$. The surface force density \vec{f}^s in the third term acts as a Lagrange multiplier that enforces the boundary conditions at the sample surface S . For a fixed defect configuration, the displacements $\vec{u}(\vec{r})$ are determined from $\delta V_t / \delta \vec{u} = 0$, which defines mechanical equilibrium

$$C_{ijkl} u_{kl,j}(\vec{r}) = -f_i(\{\vec{r}^\alpha\}, \vec{r}), \quad \vec{r} \text{ in } V, \quad (6)$$

and the boundary condition at the surface of the elastic material

$$C_{ijkl} u_{kl}(\vec{r}) n_j(\vec{r}) = f_i^s(\vec{r}), \quad \vec{r} \text{ on } S, \quad (7)$$

where \vec{n} is the outward directed surface normal of the surface element dS . By combining Eq. (6) and Eq. (4), one finds $V_e = \frac{1}{2} \int d^3r f_i u_i = -\frac{1}{2} V_d$. Therefore the overall energy $V_t = V_d + V_e = \frac{1}{2} V_d = -V_e$ and the overall energy can be written as function of the defect configuration only. In this way, the *direct* interactions of the particles with the medium can be rigorously transformed into an *indirect* interaction between defects. This also allows the calculation of the interaction of a single defect with a boundary-induced strain field or an external strain field applied at the boundary. The ground-state configuration of elastically interacting defects is obtained by minimizing total energy V_t .

C. Interaction between active cells and an elastic medium

The forces exerted by mechanically active cells on the environment are mainly due to actomyosin contractility. Thus, in contrast to the interaction of physical force dipoles with the elastic medium, where the force can be derived from conventional interaction potentials, cellular forces are continuously and actively generated by the cell and involve non-equilibrium processes that are tightly regulated by biochemical events inside the cell. Hence, the interactions of cells with an elastic environment are more complicated than for physical defects and there is little *a priori* reason why they should be described by Eq. (2). Motivated by recent experiments with elastic substrates [11–13], we have argued before that despite these complications, a similar description as for the physical case can be employed for the cellular one [31]. We asked which kind of information a cell can extract from its elastic environment using its contractile machinery and suggested that an appropriate scalar quantity to characterize the environment is the work the cell has to perform in order to build up a certain level of force against the elastic environment. Experimental observations suggest that active cell behavior amounts to a simple preference for large effective stiffness, which corresponds to a minimization of this energy. As a simple analog, consider a linear spring. In order to build up a certain force F , the energy $W = Kx^2/2 = F^2/2K$ has to

be invested into the spring, where x is displacement and $F = Kx$ is force at equilibrium. If there is a choice of different springs with different spring constants K , the smallest amount of energy W to build up F has to be invested into the spring with the largest value for K . In the case of cells, the different springs correspond to different directions as probed by different stress fibers, and on the long run, the cell will orient in that direction that corresponds to the largest value of K , possibly because in this direction, the buildup of force is most efficient. The example of the linear spring can also be used to illustrate the main difference to the physical case, when the final configuration is determined by the overall energy $V_i = Kx^2/2 - Fx = -F^2/2K = -W$. Thus in contrast to the case of cellular force dipoles for physical dipoles minimal values of stiffness K are most favorable.

We now explain our reasoning in more detail for the case of cells in a three-dimensional environment described by continuum elasticity theory. In order to identify a suitable analog to the spring constant K , we introduce the concept of *local effective stiffness* of the elastic environment. We define this quantity to be the work W required to build up a unit force in the elastic medium. The deformation work W required to build up an arbitrary force distribution $\vec{f}(\vec{r})$ is given by

$$W = \int d^3r \int_0^{\vec{f}} C_{ijkl} u_{kl}(\vec{r}) du_{ij}(\vec{r}), \quad (8)$$

which in the absence of external prestrain is equivalent to the energy stored in the elastic medium given in Eq. (4). Then integration by parts gives

$$W = -\frac{1}{2} \int d^3r u_i(\vec{r}) C_{ijkl} u_{kl,j}(\vec{r}) + \frac{1}{2} \oint dS_n C_{ijkl} u_{kl}(\vec{r}) u_i(\vec{r}). \quad (9)$$

Applying the mechanical equilibrium conditions of the elastic medium, Eqs. (6) and (7), yields

$$W = \frac{1}{2} \int d^3r u_i(\vec{r}) f_i(\vec{r}) + \frac{1}{2} \oint dS u_i(\vec{r}) f_i^s(\vec{r}). \quad (10)$$

In an infinite medium the boundary condition at the surface yields a vanishing surface integral. Hence for a force distribution centered around \vec{r} , the volume integral can be turned into a local expression by using the definitions of Eq. (1):

$$W^\infty = \frac{1}{2} \int f_i(\vec{r} + \vec{s}) u_i(\vec{r} + \vec{s}) d^3s = \frac{1}{2} \sum_{n=0}^{\infty} \frac{1}{n!} P_{i_1, \dots, i_n} u_{i_1, i_1, \dots, i_n}(\vec{r}). \quad (11)$$

In particular, for a force monopole and a force dipole one finds $W^\infty = \frac{1}{2} P_i u_i^\infty(\vec{r})$ and $W^\infty = \frac{1}{2} P_{ij} u_{ij}^\infty(\vec{r})$, respectively, where \vec{u}^∞ and u_{ij}^∞ are the displacement and strain tensor fields caused by the respective force multipole in an infinite

homogeneous medium. W^∞ relates the effective stiffness encountered by a cell to the elastic constants. Since strain scales inversely with elastic constants, W^∞ decreases if the elastic constants increase. For an elastically anisotropic medium, W^∞ varies with the direction of force application, which provides an orientational clue for cell orientation. As we will see below, tensile prestrain or boundary-induced tensile image strain also leads to an increased effective stiffness. Therefore minimization of W^∞ corresponds to the experimentally observed cellular preference for large effective stiffness.

D. Isotropic elastic medium

The mechanical equilibrium condition, Eq. (6), states that the applied body forces $f_i(\vec{r})$ are balanced by the internal restoring forces $\sigma_{ij,j}(\vec{r})$, where $\sigma_{ij}(\vec{r}) = C_{ijkl} u_{kl}(\vec{r})$ is the stress tensor. In the following, we will consider only isotropic elastic materials, that is, there are two elastic constants, e.g., the Lamé coefficients μ and λ or Young modulus E (elastic rigidity) and Poisson ratio ν (that describes the relative importance of shear and compression modes). For our purpose, it is convenient to define a third pair of elastic constants, $\Lambda = \lambda/\mu$ and $c = 2\mu + \lambda = \mu(2 + \Lambda)$. Therefore Poisson ratio $\nu = \Lambda/(2\Lambda + 1)$ and $\nu = 1/2, 1/4$, and 0 correspond to $\Lambda \rightarrow \infty, \Lambda = 1$, and $\Lambda = 0$, respectively. In practice, E will be of the order of a few kilopascal, which is a typical value for physiological tissues (simple scaling shows that for a typical force $F = 10$ nN at focal adhesions, a deformation in the micrometer range corresponds to $E = 10$ kPa). Values for the Poisson ratio ν are close to $1/2$ (incompressible medium) both for synthetic elastic substrates and physiological hydrogels. However, other values for ν might be realized in future applications, e.g., for artificial tissues or on compliant surfaces of biosensors. For isotropic elasticity, the elastic constant tensor of the medium reads $C_{ijkl} = \lambda \delta_{ij} \delta_{kl} + 2\mu \delta_{ik} \delta_{jl}$ and Eq. (6) is conveniently rewritten using a vector notation as

$$\Delta \vec{u}(\vec{r}) + (1 + \Lambda) \vec{\nabla} \vec{\nabla} \cdot \vec{u}(\vec{r}) = -\frac{\vec{f}(\vec{r})}{\mu}, \quad \vec{r} \text{ in } V, \quad (12)$$

which is a linear second order differential equation for the displacement field and has to be solved with the appropriate boundary conditions.

Since the differential equation, Eq. (12), is linear, the superposition principle applies and the boundary value problem is formally solved by determining the Green tensor $G_{ij}(\vec{r}, \vec{r}')$, i.e., the kernel for a pointlike body force $f_i(\vec{r}) = f_i \delta(\vec{r} - \vec{r}')$. The elastic fields of more complicated force distributions can be obtained by convolution of the Green tensor with the force density, i.e., $u_i(\vec{r}) = \int G_{ij}(\vec{r}, \vec{r}') f_j(\vec{r}') d^3r'$. The elastic fields resulting from force dipoles are obtained by differentiation of G_{il} , $u_i(\vec{r}) = G_{il,k}(\vec{r}, \vec{r}') P_{kl}$ and $u_{ij}(\vec{r}) = G_{il,kj}(\vec{r}, \vec{r}') P_{kl}$. In general, the determination of Green functions in elasticity theory for a given geometry and boundary condition is rather difficult, since the second term in Eq. (12) couples different components of the displacement field. By taking the Laplacian of

Eq. (12), one arrives at the biharmonic equation $\Delta\Delta\vec{u}=0$ for the displacements. Thus, harmonic potential theory is frequently used, for instance, in the stress function χ method [34] and in the Galerkin-vector approach [35], in addition to other methods like expansion of \vec{u} in terms of a suitable complete basis set of orthonormal functions [36].

E. External strain

We now consider how a cell establishes a force pattern in a prestrained homogeneous medium. The work required to generate a force pattern in the presence of an externally imposed strain tensor field $u_{ij}^e(\vec{r})$ is given by

$$W = \int d^3r \int_0^{u_{ij}^e + u_{ij}^{\vec{f}}} C_{ijkl} u_{kl}(\vec{r}) du_{ij}(\vec{r}) - \int d^3r \int_0^{u_{ij}^e} C_{ijkl} u_{kl}(\vec{r}) du_{ij}(\vec{r}) = W^\infty + \Delta W^e \quad (13)$$

with

$$\Delta W^e = \int d^3r C_{ijkl} u_{ij}^{\vec{f}} u_{kl}^e(\vec{r}) = \sum_{n=0}^{\infty} \frac{1}{n!} P_{i_1, \dots, i_n} u_{i_1, \dots, i_n}^e(\vec{r}). \quad (14)$$

The derivation of Eq. (14) proceeds along the same lines as for Eq. (11). In particular, for a single force dipole one gets $\Delta W^e = P_{ij} u_{i,j}^e(\vec{r})$. Because of contractile cell activity, P_{ij} has negative eigenvalues ($P < 0$). Thus, tensile prestrain ($u_{ij}^e > 0$) decreases W as does a larger rigidity E and hence is interpreted by the cell as an increase in effective stiffness (*strain stiffening*). In contrast, compressive prestrain corresponds to a decrease in effective stiffness and hence is avoided by the cell.

F. Boundary-induced image strain

We now consider the energy involved to deform an elastic medium in the presence of a sample boundary. In order to quantify the effect introduced by the boundary, we split $u_{ij} = u_{ij}^\infty + u_{ij}^b$ into a contribution arising in an infinite medium u_{ij}^∞ and a boundary-induced strain field u_{ij}^b (*image strain*) that depends on sample geometry and boundary condition. u_{ij}^∞ ensures that the force balance is satisfied everywhere in the sample volume V . However, u_{ij}^∞ will not satisfy the boundary condition at S that requires one to introduce u_{ij}^b . In order to keep the force balance in the sample, the image displacements have to be homogeneous solutions of Eq. (12). Otherwise they can be chosen in such a way that the boundary conditions are satisfied. Now $W = W^\infty + \Delta W^b$, where W^∞ is the energy of the infinite medium and ΔW^b is the additional energy due to the boundary effect. For the latter, we have

$$\Delta W^b = \frac{1}{2} \int d^3r f_i(\vec{r}) u_i^b(\vec{r}) + \frac{1}{2} \oint dS f_i^s(\vec{r}) u_i(\vec{r}), \quad (15)$$

which includes both the effects of fixed boundary strain and fixed boundary forces. In principle, the boundary conditions

in a physiological context can be very complicated. In our calculations we will restrict ourselves to two fundamental reference cases, namely, *free boundaries*, where the normal tractions vanish at the boundary, i.e., $f_i^s(\vec{r}) = 0$, and *clamped boundaries*, where the displacements vanish at the boundary, i.e., $u_i(\vec{r}) = 0$. We will refer to the former as the *Neumann problem* and to the latter as the *Dirichlet problem*. In both cases, the surface integral in Eq. (15) vanishes. Thus, the change in effective stiffness induced by a boundary as encountered by a force dipole reads $\Delta W^b = \frac{1}{2} P_{ij} u_{i,j}^b(\vec{r})$. In this way, cells can actively sense not only the presence of a close-by surface, but also its shape and boundary condition.

G. Elastic interactions of cells

Strain fields produced by other cells may be large enough to be detected as external strain by the cell, which gives rise to an elastic interaction of cells. Even if cells have initially isotropic force patterns, they will sense anisotropic strain and begin to polarize. The change in stiffness encountered by a force pattern \vec{f} centered around \vec{r} caused by a second force pattern \vec{f}' centered at \vec{r}' reads

$$\begin{aligned} \Delta W^{\vec{f}\vec{f}'} &= \int d^3s f_i(\vec{r} + \vec{s}) u_i(\vec{r} + \vec{s}) \\ &= \int \int d^3s d^3s' f_i(\vec{r} + \vec{s}) G_{ij}(\vec{r} + \vec{s}, \vec{r}' + \vec{s}') f_j'(\vec{r}' + \vec{s}') \\ &= \sum_{n=0}^{\infty} \sum_{m=0}^{\infty} \frac{1}{n!} \frac{1}{m!} P_{i_1, \dots, i_n} G_{ij, i_1, \dots, i_n j_1, \dots, j_m} \\ &\quad \times (\vec{r}, \vec{r}') P'_{j_1, \dots, j_m}, \end{aligned} \quad (16)$$

where the indices i_1, \dots, i_n denote derivatives of the Green function with respect to the unprimed coordinates and j_1, \dots, j_m derivatives with respect to the primed coordinates. For translationally invariant geometries, for instance, in infinite space, $G_{ij}(\vec{r}, \vec{r}') = G_{ij}(\vec{r} - \vec{r}')$ and derivatives for j_k become equivalent to derivatives for $-i_k$. As a model for elastically interacting cells, we consider how identical, static anisotropic contraction dipoles organize in a soft medium in order to sense maximal effective stiffness in their environment. The case $n = m = 1$ in Eq. (16) corresponds to the force dipolar interaction:

$$\Delta W^{PP'} = P_{li} u_{i,l}(\vec{r}) = P_{li} G_{ij, lk}(\vec{r}, \vec{r}') P'_{kj} \quad (17)$$

and will be discussed in more detail below.

H. Summary modeling section

To summarize the first part of this paper, both physical defects and active cells respond to elastic deformations in their environment and we suggest that the same mathematical formalism can be used to describe both situations. In fact, all formulas derived in this section for interactions of cells with external strain, sample boundaries and other cells as quantified by W describe the corresponding interactions of physical dipoles as quantified by V_l , with W and V_l being

related to each other simply by a switch in sign. This result is typical for situations described by energies with quadratic scaling, as explained above for the simple case of a linear spring. For different situations of interest we found the same result $\Delta W = P_{ij}u_{ij}$, where u_{ij} is the strain tensor evaluated at the position of the force dipole P_{ij} . Depending on the situation of interest, this strain tensor can correspond to externally imposed strain, image strain induced by a sample boundary or strain due to the traction of other force dipoles. Our formula shows that cells can sense anisotropies in their environment only through an anisotropic probing process: if the probing process were isotropic, $P_{ij} = P\delta_{ij}$, we would find $W = Pu_{ii}$ and cells could only sense the scalar quantity u_{ii} describing the local relative change in volume, but not any tensorial quantity like the direction of external strain.

It is important to note that the above equations for active cells are not interaction potentials in a strict physical sense. Rather these equations try to quantify information that cells can gain by pulling on their environment and show how external perturbations result in changes in effective stiffness. The experimental observation that active cells prefer large effective stiffness in their environment leads to the interaction laws for cells given in Eqs. (14)–(16). In this way, we can predict cellular self-organization in soft media from an extremum principle in elasticity theory, in excellent agreement with experimental results [31]. The structure formation for physical dipoles follows simply by inverting the sign of the interaction laws derived for active cells. This case might also apply to artificial or inert cells [29]. For biomimetic systems, one might think of vesicles or nanocapsules which contract on adhesion to an elastic environment. For cellular systems, one might think of cells which are deficient in regard to the experimentally observed dynamic response of normal cells to elastic properties of the environment.

In regard to modeling of active cells, we assume that they probe their elastic environment through an anisotropic process in which force is of central importance, and that this process results in a cellular preference for large effective stiffness in the environment. Although the phenomena described here are closely related to cell morphology and the dynamics of focal adhesions, these aspects are not the subject of the present work. In particular, the magnitude P of the cellular force dipole tensor does not enter our predictions, in contrast to the positions and orientations represented by the dipole tensor P_{ij} . This reflects the fact that our model focuses on the extracellular properties that can be sensed by the cell. Since we avoid modeling cell morphology and dynamics of focal adhesions, we are able to describe the active behavior of cells in the same mathematical framework developed before to describe physical defects in a deformable medium. In particular, both cases require the solution of the corresponding elastic boundary value problem given in Eqs. (6) and (7). In the following section, we present exact solutions for different cases of interest.

III. EXAMPLES OF CELL ORGANIZATION

A. Interaction with external strain

As an example for cell organization in a prestrained environment, we consider a homogeneously prestrained

elastic slab with an uniaxial stress p acting along the z axis. The other faces are traction free, i.e., the stress tensor has only one nonzero component $\sigma_{zz} = p$. Then the corresponding strain tensor has only diagonal components $u_{ij}^e = p/E\{(-\nu, 0, 0), (0, -\nu, 0), (0, 0, 1)\}$ independent of position. Contraction of this external strain tensor with the force-dipole tensor P_{ij} according to Eq. (14) leads to

$$\Delta W^e = \frac{pP}{E}[(1 + \nu)\cos^2\theta - \nu], \quad (18)$$

where θ is the orientation of the dipole relative to the direction of externally applied strain. Equation (18) applies to both a cell on the top surface of the strained slab (elastic substrate) or inside a strained infinite elastic material (hydrogel). For tensile stress ($p > 0$) the cell senses maximal effective stiffness along the direction of stretch $\theta = 0$, thus cells orient preferentially in the direction of stretch in a prestrained environment.¹ On the other hand, due to lateral contraction, cells in a precompressed environment ($p < 0$) will orient perpendicularly to the axis of compression, which is a combined effect of compressive strain avoidance in the z direction and maximal tensile strain detection in the perpendicular directions, which will be most pronounced for incompressible media ($\nu \approx 1/2$). In contrast, a physical anisotropic contraction dipole, causing a local contraction of the environment along its axis, is repelled (attracted) by tensile (compressive) strain, because the negative interaction energy with the medium is reduced (increased) due to the expansion (compression) of the environment caused by the external field. Physical anisotropic contraction dipoles therefore orient in the opposite way as mechanosensing cells with respect to external homogeneous strain.

B. Dipoles on elastic half space

Mechanically active cells adhering to an elastic substrate can interact elastically with each other according to Eq. (16). If the thickness of the substrate is much larger than the elastic displacements on the top surface, it can be modeled as a semi-infinite elastic space [6]. The Green function for a force applied to the surface of a semi-infinite space is given by the well-known Boussinesq solution [34]. Since tangential forces are expected to be much larger than normal forces, P_{ij} can be restricted to the x - y plane. Moreover, the normal displacement component contributes very little to the elastic interaction and we may use the two-dimensional (2D) Green function, i.e., only the x - and y -components of the Boussinesq solution

$$G_{ij}^{2D}(\vec{r}, \vec{r}') = a_1 \left\{ a_2 \delta_{ij} + \frac{R_i R_j}{R^2} \right\} \frac{1}{R}, \quad (19)$$

where $\vec{r} = \vec{r} - \vec{r}'$ and

$$a_1 = \frac{\Lambda(\Lambda + 2)}{4\pi c(1 + \Lambda)} = \frac{\nu(1 + \nu)}{\pi E}, \quad a_2 = \frac{2 + \Lambda}{\Lambda} = \frac{1 - \nu}{\nu}. \quad (20)$$

¹In Ref. [31], tensile stress has been defined with an opposite sign, resulting in an opposite sign in Eq. (18).

It is convenient to define the angles θ , θ' , and α via the scalar products $\cos \theta = \vec{l} \cdot \vec{r}$, $\cos \theta' = \vec{l}' \cdot \vec{r}$, and $\cos \alpha = \vec{l} \cdot \vec{l}'$. Then the change in effective stiffness encountered by one cell due to the traction of the other is given by

$$\Delta W^{PP'} = a_1 \frac{PP'}{2R^3} f(\theta, \theta', \alpha) \quad (21)$$

with the angular dependence

$$f(\theta, \theta', \alpha) = 3(\cos^2 \theta + \cos^2 \theta' - 5 \cos^2 \theta \cos^2 \theta' - \frac{1}{3}) - (1 - a_2) \cos^2 \alpha - 3(a_2 - 3) \cos \alpha \cos \theta \cos \theta'. \quad (22)$$

Since the displacements of a force-dipole scale $\sim R^{-2}$, the strain field scales $\sim R^{-3}$ with distance, which leads to a long-ranged elastic interaction ($W^{PP'} \sim R^{-3}$) typical for dipolar interactions. The complicated angular dependence in Eq. (22) results in a highly anisotropic interaction. Note that for the planar geometry, there are only two independent angles. Nevertheless here we prefer to write the interaction symmetric in the primed and unprimed coordinates, since this is favorable for numerical implementations.

$\Delta W^{PP'}$ has a pronounced minimum for aligned dipoles ($\theta = \theta' = \alpha = 0$), independent of ν . A contractile cell causes a local compression of the substrate underneath the cell along the contraction axis and tensile strain at more distant points. Hence at distant points maximal strain stiffening occurs along the axis of contraction. A second cell will therefore upregulate its mechanical activity along the same direction. This scenario constitutes a positive mechanical feedback loop for cell alignment, since in the aligned configuration the mechanical activity of one cell upregulates the activity of the other and vice versa. At low cell densities, a common pattern for the organization of elastically interacting cells will therefore be the formation of strings of cells, similar to the case of electric dipoles [37]. Strings might close into rings so that each cell is fully activated by its neighbors.

The 2D case for physical dipoles has been discussed before for the isotropic case [24]. Then

$$V_t = -P \delta_{li} G_{ij, lk}(\vec{r}, \vec{r}') P' \delta_{kj} = -PP' G_{ij, ij}(\vec{r}, \vec{r}') = \frac{(2 + \Lambda)^2 PP'}{4 \pi (1 + \Lambda) c R^3}. \quad (23)$$

Thus, for identical dipoles the interaction is isotropic and repulsive. The case of anisotropic physical dipoles is described by the negative of Eq. (21). Then the ground-state configuration strongly depends on the Poisson ratio ν via the angular dependence of Eq. (22). For incompressible media, $\nu = 1/2$ ($\Lambda \rightarrow \infty$), dipoles arrange with perpendicular orientations in a local T configuration. This leads to rather compact structure formation, with a square lattice pattern at intermediate and a herringbone pattern at high dipole densities, similar to the situation with electric quadrupoles [29]. For highly compressible media, $\nu \rightarrow 0$ ($\Lambda \rightarrow 0$), dipoles prefer to align side by side in a railway tracklike configuration. For $\nu = 1/5$

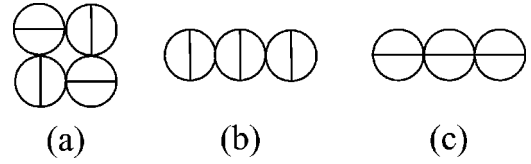


FIG. 2. Different structures arising from elastic interactions of anisotropic force dipoles on top of an elastic half space. (a) Physical force dipoles for Poisson ratio $\nu \approx 1/2$ locally form a T configuration. The resulting structure formation is compact and similar to the one of electric quadrupoles. (b) Physical force dipoles for Poisson ratio $\nu \approx 0$ align side by side in a railway tracklike configuration. The crossover between (a) and (b) occurs at $\nu = 1/5$. (c) Cellular force dipoles align in strings, similar to electric dipoles and independent of the value for ν .

($\Lambda = 2/3$), both states have degenerate energies. Figure 2 schematically shows the different structures predicted by our analysis.

C. Dipoles in elastic full space

Strain propagation in an elastic 3D infinite medium is described by the Thomson Green function [34]

$$G_{ij}^\infty(\vec{r}, \vec{r}') = a_1^\infty \left\{ a_2^\infty \delta_{ij} + \frac{R_i R_j}{R^2} \right\} \frac{1}{R}, \quad (24)$$

with

$$a_1^\infty = \frac{1 + \nu}{8 \pi E (1 - \nu)} = \frac{\Lambda + 1}{8 \pi c}, \quad a_2^\infty = (3 - 4\nu) = \frac{3 + \Lambda}{1 + \Lambda}. \quad (25)$$

The most important result for physical dipoles is the fact that since $G_{ii}^\infty = 0$, the elastic interaction of isotropic dipoles in 3D vanishes [22]. Therefore their interaction is completely determined by boundary-induced interactions, like for hydrogen in metal samples of finite size [23].

For the elastic interaction of two active cells, we find

$$\Delta W^{PP'} = a_1^\infty \frac{PP'}{2R^3} f^\infty(\theta, \theta', \alpha) \quad (26)$$

with the angular function $f^\infty(\theta, \theta', \alpha)$ given by Eq. (22) by replacing the constants a_1 and a_2 with a_1^∞ and a_2^∞ , respectively. Note that in 3D there are three independent orientational degrees of freedom. In Fig. 3 we show a density plot of $\Delta W^{PP'}$ for dipoles with relative orientations $\alpha = 0$ and $\alpha = \pi/2$ positioned in the x - z plane for two different values of the Poisson ratio, $\nu = 0$ and $\nu = 1/2$. Like on 2D substrates, cells in a 3D environment encounter a mechanical feedback loop favoring cell alignment. For two parallel dipoles in z direction placed along the z axis, we find

$$\Delta W^{PP'} = -\frac{(\Lambda + 2)P^2}{2 \pi c} \left(\frac{1}{z} \right)^3, \quad (27)$$

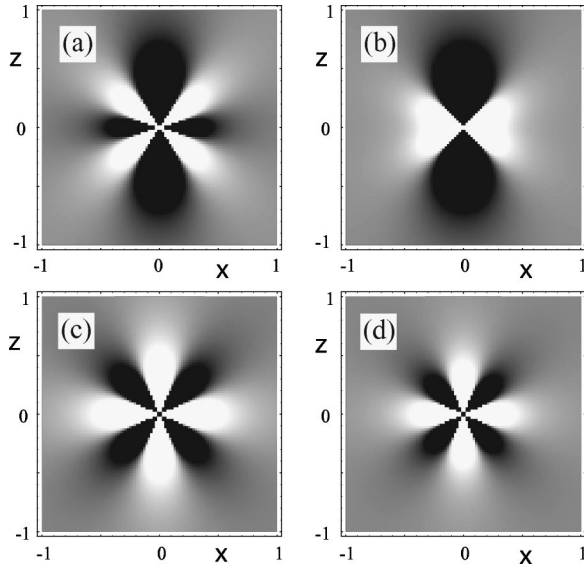


FIG. 3. Density plots of cellular interaction potential $\Delta W^{PP'}$ from Eq. (26) for (a,b) parallel and (c,d) perpendicular orientations. In (a,c), Poisson ratio $\nu=1/2$, and in (b,d), $\nu=0$. One dipole oriented along the z axis is fixed at the origin, while the other is moved in space. Black denotes areas of attraction and white areas of repulsion. The interaction potential for physical force dipoles simply differs in sign, thus black and white exchange meaning. (a,b) Independent of the value for ν , two cells prefer alignment (black region along z axis). The interaction in the railway track configuration (along x axis) changes sign at $\nu=1/4$, when the black cone vanishes. (c,d) The T configuration is the ground state for physical dipoles in 3D independent of the value for ν (white regions along z and x axes). This is different on an elastic half space, in which case the ground state changes from the T to the railway track configuration for $\nu=1/5$.

which yields the optimal configuration independent of the value for Λ (or, equivalently, ν). Again this behavior is similar to the ones of the electric dipoles [37]. For two parallel dipoles in z direction placed along the x axis (railway track configuration), we find

$$\Delta W^{PP'} = \frac{(\Lambda - 1)P^2}{8\pi c} \left(\frac{1}{x}\right)^3. \quad (28)$$

Thus $\Delta W^{PP'}$ changes sign as Λ varies through 1 ($\nu=1/4$). Finally, in the T configuration, where the first dipole is fixed in z direction at the origin and the second dipole is positioned in the x - y plane oriented perpendicular to the z axis, we find

$$\Delta W^{PP'} = -\frac{(\Lambda + 1)P^2}{4\pi c} \left(\frac{1}{r}\right)^3, \quad (29)$$

which is always positive and yields a globally maximal $\Delta W^{PP'}$. Therefore it corresponds to a globally minimal $V_t = -\Delta W^{PP'}$ and the T configuration is the ground state of two physical anisotropic contraction dipoles, independent of the value for ν . The aggregation of physical dipoles in 3D is more complicated than in 2D, since the T configuration

cannot be continued in 3D without causing frustration. This leads to the existence of many metastable states.

D. Dipoles in elastic half space

The elastic isotropic half space with a clamped surface at $r_3=0$ constitutes a Dirichlet problem with vanishing displacements at the planar boundary, $u_i(\vec{r})=0$ for $r_3=0$, whereas the free surface leads to a Neumann boundary value problem with vanishing surface tractions, $\sigma_{ij}(\vec{r})n_j=0$ for $r_3=0$ with $\vec{n}=(0,0,1)$ being the surface normal. The boundary value problem of the semi-infinite space can be solved using the concept of image singularities. Image approaches are well known from electrostatics; the simplest example is the charge in front of a metal plate. Here, the field due to a charge Q at $\vec{r}'=(r'_1, r'_2, r'_3)$ with the boundary at $r_3=0$ is equivalent to the field of the charge and an image charge $-Q$ at $\vec{r}'_{\text{im}}=(r'_1, r'_2, -r'_3)$ without a boundary. In analogy, the displacement field due to a unit force at \vec{r}' close to a planar surface of a semi-infinite space is equivalent to the superimposed fields of a set of force nuclei placed in a homogeneous infinite substrate, i.e.,

$$G_{ij}(\vec{r}, \vec{r}') = G_{ij}^{\infty}(\vec{r}, \vec{r}') + G_{ij}^{\text{im}}(\vec{r}, \vec{r}'), \quad (30)$$

where G_{ij}^{∞} is the Green function in an infinite medium, Eq. (24), and G_{ij}^{im} specifies its image system, which is a sum of functions derived from G_{ij}^{∞} by differentiation (point images, i.e., forces and force dipoles) or integration (line images, i.e., a line of force nuclei). Despite its rather simple geometry, the image system of the elastic half space is rather complicated and consists of up to 15 image nuclei, including point nuclei located at $\mathbf{r}'_{\text{im}}=(r'_1, r'_2, -r'_3)$ and line images running normal to the surface and extending from $-r'_3$ to infinity. The image system of the free half space was calculated by Mindlin using a Boussinesq-Galerkin representation [35]. The Green function of the clamped half space has been derived by Phan-Thien applying a Papkovitch-Neuber ansatz, however without revealing the image system in detail [38]. Quite recently, Walpole [39] used methods of general harmonic potential theory and presented the image system for two joined half spaces, which includes the clamped or free half space as limiting cases of infinite or vanishing shear rigidity in one of the joined spaces. Introducing the harmonic function

$$\frac{1}{s} = \frac{1}{|\vec{r} - \vec{r}'_{\text{im}}|}, \quad (31)$$

where s the distance from the image point, and

$$\begin{aligned} \Phi &= \ln(r_3 + r'_3 + s), \\ \Psi &= (r_3 + r'_3)\Phi - s, \end{aligned} \quad (32)$$

the image Green tensor G_{ij}^{im} of the isotropic elastic half space reads [39]:

$$\begin{aligned}
 G_{ij}^{\text{im}}(\vec{r}, \vec{r}') = & MG_{ij}^{\infty}(\vec{r}, \vec{r}'_{\text{im}}) + \frac{Jr'_3(1+\nu)}{4\pi E(1-\nu)} \left\{ s_{,ij3} - 2\delta_{j3}s_{,i33} \right. \\
 & - 4(1-\nu)\delta_{i3} \left[\left(\frac{1}{s} \right)_{,j} - 2\delta_{j3} \left(\frac{1}{s} \right)_{,3} \right] \left. \right\} \\
 & - \frac{Jr'_3(1-2\nu)(1+\nu)}{2\pi E(1-\nu)} \delta_{j3} \left(\frac{1}{s} \right)_{,i} \\
 & - \frac{Jr'_3{}^2(1+\nu)}{4\pi E(1-\nu)} \left[\left(\frac{1}{s} \right)_{,ij} - 2\delta_{j3} \left(\frac{1}{s} \right)_{,i3} \right] \\
 & - \frac{C(1-2\nu)(1+\nu)}{4\pi E(1-\nu)} (\Psi_{,ij} - 2\delta_{j3}\Psi_{,i3}) \\
 & + \frac{B(1+\nu)}{2\pi E} \delta_{j3}\Phi_{,i} + \frac{B(1+\nu)}{2\pi E} (\delta_{i3}\Phi_{,j} - \delta_{ij}\Phi_{,3}),
 \end{aligned} \tag{33}$$

where the coefficients M , J , C , and B depend on the boundary condition (subscripts: free f , clamped c) and the Poisson ratio ν [39]:

$$\begin{aligned}
 M^f &= (3-4\nu), & M^c &= -1, \\
 J^f &= -1, & J^c &= 1/(3-4\nu), \\
 C^f &= 2(1-\nu), & C^c &= 0, \\
 B^f &= 2(1-2\nu), & B^c &= 0.
 \end{aligned} \tag{34}$$

For a fixed j , each line in Eq. (33) represents the i th component of the displacement field of one fundamental strain nuclei of an infinite medium. For a free surface, five image singularities contribute to a surface tangential or normal force component. A tangential force $j=1,2$ introduces, in the order of lines of Eq. (33), three point images (force, double force with moment and a doublet) and two line images (line of doublets and line of double forces with moment) [35]. A normal force $j=3$ induces four point images (force, double force, doublet, center of compression/dilation) and a line of compression/dilation centers [35]. In a clamped half space the line images disappear ($B=C=0$) and there are only the three or four point images for a tangential or normal force component, respectively. Interestingly, the strength of the higher order point singularities is proportional to the distance r'_3 of the source point from the surface. Hence their relative contribution to the displacement field with respect to the image force increases with increasing distance of the source force from the surface. Note that for $r'_3 \rightarrow 0$, i.e., for a force acting at a free surface of a semi-infinite space, Eq. (33) yields the Boussinesq Green function from Eq. (19) for tangentially applied forces and the solution of Cerruti for normally applied forces. The dominant terms to the image displacement field far away from the surface arise from the image force and the line images $\sim 1/s$, followed by the dipole type defects (double force, compression center) $\sim r'_3/s^2$ and finally the doublet $\sim r'_3{}^2/s^3$. The Poisson ratio ν changes

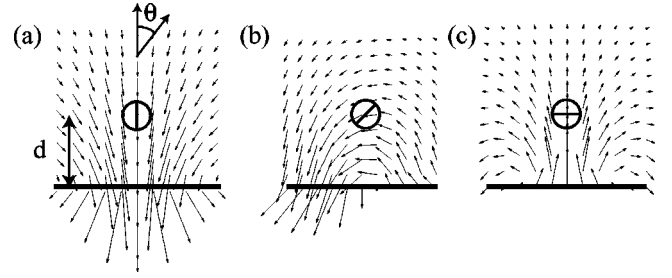


FIG. 4. Image fields \vec{u}^b for a contraction dipole P_{ij} positioned at $\vec{r}' = (0,0,d)$ in front of a clamped surface of a semi-infinite space for Poisson ratio $\nu=1/2$. Dipole orientations are (a) $\theta=0$, (b) $\theta=\pi/4$, and (c) $\theta=\pi/2$ with respect to the surface normal. At the clamped surface the image displacements \vec{u}^b balance the displacements \vec{u}^∞ of an infinite space. Inside the sample, they are homogeneous solutions of the elastic equations. The interaction of a dipole with the clamped surface is equivalent to the interaction of the dipole with a set of image singularities placed at $\vec{r}'_{\text{im}} = (0,0,-d)$. For a free surface, the normal tractions vanish and all image displacements change sign. For $\nu < 1/2$, there is an additional contribution to \vec{u}^b derived from line images. However, the interaction of force dipoles with the boundary does not change qualitatively as ν is varied.

the relative magnitude of the image singularities with respect to each other, but does not change their type (i.e., their sign). Therefore, strain propagation in the half space is expected to stay qualitatively similar with varying ν . Changing the boundary condition from free to clamped, the point images flip their sign, which indicates that clamped and free boundary will induce qualitatively opposite effects. Indeed, for the special case of an incompressible medium, $\nu=1/2$, clamped and free half space induce the same boundary fields but with opposing signs.

The image displacements \vec{u}^b induced by a force dipole P_{ij} at \vec{r}' are obtained from Eq. (33) by differentiation with respect to the primed coordinates. Note that the planar surface at $r_3=0$ breaks the translational invariance along the z axis, which means that differentiation of G_{ij}^b with respect to r_3 and r'_3 are not equivalent. Since the strength of the dipolar singularities in G_{ij}^{im} is proportional to r'_3 , taking the derivative with respect to r'_3 will lead to dipole images of r'_3 -independent strength that are proportional to the dipole strength P . Therefore, the far field image displacements produced by a force dipole in front of a planar surface are dominated by image dipole terms $\sim 1/s^2$ of strength proportional to M and J and additional images derived from the line image terms. In Fig. 4 we plot \vec{u}^b for three different dipole orientations with respect to the surface normal of a clamped half space for Poisson ratio $\nu=1/2$. In this case, all image displacements point in the opposite direction for a free surface.

According to Eq. (15), the change in effective stiffness encountered by a force dipole P_{ij} positioned a distance $r'_3 = d$ away from the surface is proportional to the induced image strain at the position of the dipole, i.e. $\Delta W^b(\vec{r}') = \frac{1}{2} P_{ij} [\partial^2 G_{ik}^{\text{im}}(\vec{r}, \vec{r}') / \partial r_j \partial r'_l] P_{kl} |_{\vec{r}=\vec{r}'}$. Because of rotational symmetry with respect to the surface normal, the surface

induced change in effective stiffness sensed by a dipole depends only on its distance d to the surface and the angle $\theta = \vec{n} \cdot \vec{l}$ between dipole orientation and surface normal. We find

$$\Delta W^b(d, \theta) = \frac{P^2}{256\pi E d^3} (a_\nu + b_\nu \cos^2 \theta + c_\nu \cos^4 \theta), \quad (35)$$

with the coefficients

$$\begin{aligned} a_\nu^f &= \frac{(1+\nu)[5+2\nu(6\nu-1)]}{1-\nu}, \\ a_\nu^c &= -\frac{(1+\nu)[15+32\nu(\nu-1)]}{(1-\nu)(3-4\nu)}, \\ b_\nu^f &= \frac{(1+\nu)[22+4\nu(2\nu-9)]}{1-\nu}, \\ b_\nu^c &= -\frac{(1+\nu)(34+32\nu^2-72\nu)}{(1-\nu)(3-4\nu)}, \\ c_\nu^f &= \frac{(1+\nu)[13(1-2\nu)+12\nu^2]}{1-\nu}, \\ c_\nu^c &= -\frac{(1+\nu)(7-8\nu)}{(1-\nu)(3-4\nu)}, \end{aligned} \quad (36)$$

being rational function of the Poisson ratio ν . ΔW^b scales quadratically in P , because the image strain scales linearly in P , in other words, the force dipole interacts with its own images. The interaction of the force dipole with the surface is a long-ranged effect and scales like a dipole-dipole interaction potential, that is, $\sim d^{-3}$. For free and clamped surfaces, all coefficients in Eq. (36) are positive and negative, respectively, irrespective of ν . Therefore, the preferred cell orientation close to the surface, i.e., the configurations of minimal ΔW^b , are parallel ($\theta = \pi/2$) and perpendicular ($\theta = 0$) orientation for free and clamped boundaries, respectively. In Fig. 5 we plot the angular dependence of ΔW^b for $\nu = 1/2$ and $\nu = 0$.

Since $|\Delta W^b| \sim 1/d^3$ increases if d decreases, the overall mechanical activity of a cell increases towards a clamped surface ($\Delta W < 0$), but decreases towards a free surface ($\Delta W > 0$). Thus we predict that cells preferentially locomote towards a clamped boundary, but tend to migrate away from a free boundary. In general, free and clamped boundaries have always opposite effects. One may think of a clamped (free) surface as the interface between the medium and an imaginary medium of infinite (vanishing) rigidity, which effectively rigidifies (softens) the medium towards the boundary. Thus for clamped (free) boundary conditions, the cell senses maximal stiffness towards (away) from the boundary. For clamped boundaries, mechanical activity of cells is favored and cells can amplify this effect by adjusting orientation. For free boundaries, mechanical activity of cells is disfavored and the orientation response is an aversion response.

For the interaction of a physical dipole with the surface, we simply have to switch sign in Eq. (35). Hence, physical

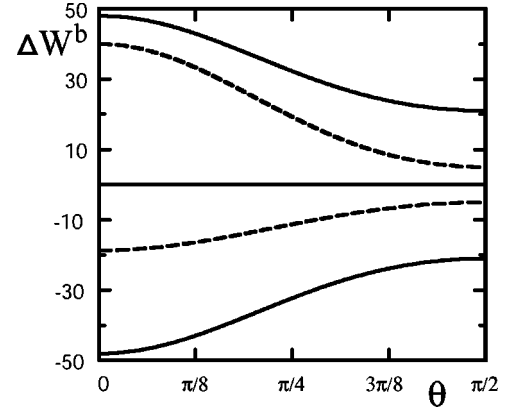


FIG. 5. Angular dependence of image interaction with the boundary, ΔW^b from Eq. (35), for a cellular force dipole positioned a distance d away from the surface of an elastic half space, plotted in units of P^2/Ed^3 and rescaled by $1/256\pi$. Curves above and below the θ axis correspond to free and clamped boundaries, respectively. Solid and dashed lines correspond to $\nu = 1/2$ and $\nu = 0$, respectively (all other Poisson ratios yield curves lying in between those shown). A clamped (free) surface effectively rigidifies (softens) the medium towards the surface. Hence, irrespective of the value of ν , cells close to a clamped surface prefer to orient perpendicular (ΔW^b minimal for $\theta = 0$) while cells close to a free surface prefer parallel orientation (ΔW^b minimal for $\theta = \pi/2$).

dipoles are attracted by free surface, and repelled from clamped surfaces. A clamped surface prevents the defect from displacing its environment to lower its potential energy, which results in a repulsive interaction. In contrast a free surface favors displacements close to the surface since at a free surface there exist no internal restoring forces acting normal to the surface. This results in an attractive interaction of the defect with the surface. Since $V_t \sim P^2$, the sign of P does not matter, i.e., dilation and contraction dipole interact in the same way with the surface.

E. Dipoles in elastic sphere

As an example for a finite sized sample, we consider the elastic sphere with radius R . For the elastic sphere, no image system has been constructed that solves the elastic boundary value problem and it is not clear whether such an image system exists. Nevertheless, the elastic equations for the elastic sphere can be solved analytically by applying an expansion in terms of vector spherical harmonics. This approach has been used by Hirsekorn and Siems [36] to solve the Neumann problem of an anisotropic force dipole in an elastic sphere with a free boundary. We will follow this approach also in order to solve the Dirichlet problem of a force dipole in a clamped sphere. Both results are then used to calculate the change in effective stiffness encountered by a force dipole in clamped and free spheres, respectively.

Analytical solutions to differential equations for scalar fields in spherical coordinates can be obtained by an expansion in terms of spherical harmonics, which form a complete orthonormal basis set on the unit sphere. In a similar way, the general solution to the equilibrium condition Eq. (12) for the vector field $\vec{u}(\vec{r})$ can be expressed as a sum over so-called

vector spherical harmonics (VSH)

$$\begin{aligned} \vec{u}(r, \Omega) = & \sum_{lm} f_{lm}(r) \mathbf{Y}_{l+1m}^\dagger(\Omega) + g_{lm}(r) \mathbf{Y}_{l-1m}^\dagger(\Omega) \\ & + h_{lm}(r) \mathbf{Y}_{lm}^\dagger(\Omega). \end{aligned} \quad (37)$$

Vector spherical harmonics $\mathbf{Y}_{JLM}(\Omega)$ form a complete orthonormal basis set on the unit sphere

$$\int \mathbf{Y}_{JLM}(\Omega) \mathbf{Y}_{J'L'M'}^\dagger(\Omega) d\Omega = \delta_{JJ'} \delta_{LL'} \delta_{MM'}. \quad (38)$$

They are the eigenfunctions of the angular momentum operator \mathbf{J} of a vector field as spherical harmonics Y_{lm} are the eigenfunctions of the (orbital) angular momentum L of a scalar field. \mathbf{J} is the vector sum $\mathbf{J} = \mathbf{L} + \mathbf{S}$ of the orbital momentum \mathbf{L} and the intrinsic spin \mathbf{S} . The eigenvectors of \mathbf{S} are the spherical basis vectors \mathbf{e}_α :

$$\mathbf{e}_{\pm 1} = -\frac{1}{\sqrt{2}}(\mathbf{e}_x \pm i\mathbf{e}_y), \quad \mathbf{e}_0 = \mathbf{e}_z \quad (39)$$

and represent a spin $S=1$ system. Since \mathbf{J} is an example of angular momentum addition, one can construct the VSH with the help of Clebsch-Gordon coefficients $C_{M-\alpha \alpha M}^{l \quad 1 \quad J}$ [40]

$$\mathbf{Y}_{JLM}(\Omega) = \sum_{\alpha} C_{M-\alpha \alpha M}^{l \quad 1 \quad J} Y_{lM-\alpha}(\Omega) \mathbf{e}_{\alpha}. \quad (40)$$

This implies that for a given J there are only three classes of VSH, namely, $l=J, J\pm 1$, which in retrospective justifies our ansatz Eq. (37).

In order to solve the boundary value problem, we split \vec{u} again into a contribution in an infinite substrate \vec{u}^∞ and a boundary induced field \vec{u}^b . \vec{u}^∞ is the solution to the inhomogeneous differential equation Eq. (12) with a body force density and thus ensures force balance everywhere inside the sample. For a force dipole P' located at \vec{r}' the VSH expansion of the displacement field $\vec{u}^\infty(\vec{r})$ reads for $r' < r$ [36]:

$$\begin{aligned} \vec{u}^\infty(\vec{r}) = & \frac{1}{c} \sum_{lm} \frac{\mathbf{Y}_{l+1m}^\dagger(\Omega)}{(2l+1)r^2} X_{lm}^{\alpha\beta}(\eta', \Omega') P'_\alpha{}^\beta \\ & - \frac{1}{c} \sum_{lm} \frac{\mathbf{Y}_{l-1m}^\dagger(\Omega)}{(2l+1)r^2} [3l+2+(l+1)\Lambda] \\ & \times C_{m-\alpha \alpha}^{l-1 \quad 1 \quad l} A_{l-2m}^{\alpha\beta}(\Omega') \eta'^{l-2} P'_\alpha{}^\beta \\ & - \frac{1}{c} \sum_{lm} \frac{\mathbf{Y}_{lm}^\dagger(\Omega)}{r^2} (2+\Lambda) \\ & \times C_{m-\alpha \alpha}^{l \quad 1 \quad l} A_{l-1m}^{\alpha\beta}(\Omega') \eta'^{l-1} P'_\alpha{}^\beta, \end{aligned} \quad (41)$$

where $\eta' = r'/r < 1$ and

$$A_{lm}^{\alpha\beta}(\Omega) = \sqrt{\frac{l+1}{2l+1}} C_{m-\alpha \beta}^{l+1 \quad 1 \quad l} Y_{lm-\alpha+\beta}(\Omega)$$

$$B_{lm}^{\alpha\beta}(\Omega) = \sqrt{\frac{l}{2l+1}} C_{m-\alpha \beta}^{l-1 \quad 1 \quad l} Y_{lm-\alpha+\beta}(\Omega)$$

$$\begin{aligned} X_{lm}^{\alpha\beta}(r, \Omega) = & -(3l+1+l\Lambda) C_{m-\alpha \alpha}^{l+1 \quad 1 \quad l} A_{lm}^{\alpha\beta}(\Omega) r^l \\ & + \sqrt{l(l+1)}(1+\Lambda) C_{m-\alpha \alpha}^{l-1 \quad 1 \quad l} \{B_{lm}^{\alpha\beta}(\Omega) r^l \\ & + \frac{1}{2} A_{l-2m}^{\alpha\beta}(\Omega) r^{l-2} [(2l-1) - (2l+1)r^2]\}. \end{aligned} \quad (42)$$

Sums over repeated indices are always implied except for Clebsch-Gordon coefficients. $P'^{\alpha\beta}$ is the force dipole tensor in the spherical basis set given by Eq. (39). The reciprocal basis vectors are $\mathbf{e}^\alpha = \mathbf{e}_\alpha^\dagger = (-1)^\alpha \mathbf{e}_{-\alpha}$ and the metric tensor is $g_{\alpha\beta} = (-1)^\beta \delta_{\alpha, -\beta}$. Spherical coordinates transform via the unitary operator $U_{\alpha i} = (\mathbf{e}_\alpha \cdot \mathbf{e}_i)$ into cartesian coordinates, i.e.,

$$P_{ij} = U_{\alpha i} U_{j \beta} P'^{\alpha\beta}. \quad (43)$$

In order to satisfy force balance inside the sphere volume, the boundary induced field \vec{u}^b must be a homogenous solution to Eq. (12). Thus, inserting Eq. (37) into Eq. (12), one obtains a set of differential equations for the radial functions $f_{lm}(r)$, $g_{lm}(r)$, and $h_{lm}(r)$ of the boundary induced field [36]

$$\begin{aligned} 0 = & [3l+2+(l+1)\Lambda] \left(f_{lm}'' + \frac{2}{r} f_{lm}' - \frac{(l+1)(l+2)}{r^2} f_{lm} \right) \\ & - \sqrt{l(l+1)}(1+\Lambda) \left(g_{lm}'' - \frac{2l-1}{r} g_{lm}' \right. \\ & \left. + \frac{(l-1)(l+1)}{r^2} g_{lm} \right), \end{aligned} \quad (44)$$

$$\begin{aligned} 0 = & (3l+1+l\Lambda) \left(g_{lm}'' + \frac{2}{r} g_{lm}' - \frac{l(l-1)}{r^2} g_{lm} \right) \\ & - \sqrt{l(l+1)}(1+\Lambda) \left(f_{lm}'' + \frac{(2l+3)}{r} f_{lm}' + \frac{l(l+2)}{r^2} f_{lm} \right) \end{aligned} \quad (45)$$

$$0 = h_{lm}'' + \frac{2}{r} h_{lm}' - \frac{l(l+1)}{r^2} h_{lm}. \quad (46)$$

The general solution to Eqs. (44)–(46) with a \vec{u}^b which is analytic at the sphere origin is [36]

$$f_{lm}(r) = a_{lm} \frac{3l+1+l\Lambda}{(1+\Lambda)(2l+3)} r^{l+1},$$

$$g_{lm}(r) = a_{lm} \frac{1}{2} \sqrt{l(l+1)} r^{l-1} (r^2 - R^2) + b_{lm} \frac{1}{2} r^{l-1},$$

$$h_{lm}(r) = c_{lm} r^l, \quad (47)$$

where R is the radius of the sphere and the remaining constants a_{lm} , b_{lm} , and c_{lm} must be determined by the boundary conditions at the sphere surface.

The Dirichlet problem of a clamped sphere yields

$$\vec{u}^b(R, \Omega) = -\vec{u}^\infty(R, \Omega), \quad (48)$$

i.e., the expansion coefficients a_{lm}^c etc. of the boundary induced field can be found by matching \vec{u}^∞ and \vec{u}^b at the sphere surface:

$$\begin{aligned} a_{lm}^c &= -\frac{1}{cR^3} \frac{(2l+3)(1+\Lambda)}{(2l+1)(3l+1+l\Lambda)R^l} X_{lm}^{\gamma\delta}(\rho', \Omega') P_{\gamma}^{\prime\delta}, \\ b_{lm}^c &= \frac{2}{cR^3} \frac{3l+2+(l+1)\Lambda}{2l+1} \left(\frac{\rho'}{R}\right)^{l-2} \\ &\quad \times C_{m-\gamma}^{l-1} A_{\gamma m}^{\gamma\delta} P_{l-2m}^{\gamma\delta}(\Omega') P_{\gamma}^{\prime\delta}, \\ c_{lm}^c &= \frac{1}{cR^3} (2+\Lambda) \left(\frac{\rho'}{R}\right)^{l-1} C_{m-\gamma}^l A_{\gamma m}^{\gamma\delta} P_{l-1m}^{\gamma\delta}(\Omega') P_{\gamma}^{\prime\delta}, \end{aligned} \quad (49)$$

where $\rho' = r'/R$ is the ratio of the distance r' of P' to the sphere center and the sphere radius R . For a sphere with a free surface normal stress has to vanish and the corresponding Neumann boundary condition reads

$$\sigma_{ij}^b \left(\frac{x_j}{r}\right)_{r=R} = -\sigma_{ij}^\infty \left(\frac{x_j}{r}\right)_{r=R}. \quad (50)$$

To determine a_{lm}^f , etc. one first has to calculate the stress tensor σ_{ij}^∞ and then balance the normal stress with the corresponding boundary induced stress σ_{ij}^b at $r=R$. The final result for the expansion coefficients in a free sphere is [36]

$$\begin{aligned} a_{lm}^f &= \frac{1}{cR^3} \frac{2(1+\Lambda)(2l+3)(l+2)}{(2l+1)M(l)R^l} X_{lm}^{\gamma\delta}(\rho', \Omega') P_{\gamma}^{\prime\delta}, \\ b_{lm}^f &= -\frac{1}{cR^3} \frac{2(l^2+l+1)+(2l^2+1)\Lambda}{(l-1)(2l+1)} C_{m-\gamma}^{l-1} A_{\gamma m}^{\gamma\delta} \left(\frac{\rho'}{R}\right)^{l-2} \\ &\quad \times A_{l-2m}^{\gamma\delta}(\Omega') P_{\gamma}^{\prime\delta}, \\ c_{lm}^f &= -\frac{1}{cR^3} \frac{(l+2)(2+\Lambda)}{l-1} \left(\frac{\rho'}{R}\right)^{l-1} \\ &\quad \times C_{m-\gamma}^l A_{\gamma m}^{\gamma\delta} P_{l-1m}^{\gamma\delta}(\Omega') P_{\gamma}^{\prime\delta}, \end{aligned} \quad (51)$$

with

$$M(l) = 2(l^2+1+l) + (2l^2+4l+3)\Lambda. \quad (52)$$

For both boundary conditions the image displacements scale $\sim 1/R^2$ with the sphere radius and the VSH expansion of \vec{u}^b converges as $\sim l^2(\rho\rho')^l$. Thus, higher l moments dominate if the dipole is close to the surface ($\rho' \rightarrow 1$). These are localized near the surface and decay rapidly towards the sphere center.

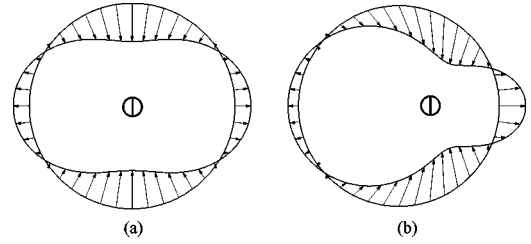


FIG. 6. Deformation of an elastic sphere ($R=1$, $\Lambda=2$, $c=1$) with a free surface by a contraction dipole oriented in the z direction. In (a) the dipole is placed at the origin, $\vec{r}=(0,0,0)$. In (b) the dipole is placed off-center at $\vec{r}=(R/4,0,0)$. The pictures show a cut through the x - z plane, but it has rotational symmetry only in (a).

We furthermore see that for a dipole close to the surface the convergence properties of the series expansion are rather poor and more l terms need to be considered to approximate the displacement field near the surface. Again clamped and free boundary induce opposing boundary fields as indicated by the opposite signs of the expansion coefficients: a clamped surface decreases \vec{u} to zero at the boundary whereas a free boundary enhances the displacements at the boundary. In Fig. 6 we plot two examples for a deformed elastic sphere with free boundaries under the action of a contraction dipole.

In order to calculate the change in effective stiffness sensed by a contraction dipole at \vec{r}' in an elastic sphere, we need to contract the gradient-displacement tensor of the boundary induced field with the dipole tensor. This is most conveniently done using the spherical representation, i.e.,

$$\Delta W^b(\vec{r}') = \frac{1}{2} P^\alpha_\beta u^b_{\alpha, \beta}(\vec{r} \rightarrow \vec{r}', \vec{r}') = \frac{1}{2} P^\alpha_\beta (e_\beta^\dagger \cdot \nabla)(e_\alpha \cdot \vec{u}^b). \quad (53)$$

Starting from the ansatz Eq. (37) for \vec{u} , $u_\alpha^\beta(\vec{r}, \vec{r}')$ can be derived by applying the gradient formula for spherical harmonics [40]

$$\begin{aligned} \nabla \Phi(r) Y_{lm}(\Omega) &= -\sqrt{\frac{l+1}{2l+1}} \left(\frac{d}{dr} - \frac{l}{r}\right) \Phi(r) Y_{l+1m}(\Omega) \\ &\quad + \sqrt{\frac{l}{2l+1}} \left(\frac{d}{dr} + \frac{l+1}{r}\right) \Phi(r) Y_{l-1m}(\Omega), \end{aligned} \quad (54)$$

and furthermore the symmetry relationships of Clebsch-Gordon coefficients [40]

$$\begin{aligned} C_{m_1 m_2 m_3}^{j_1 j_2 j_3} &= (-1)^{j_2+m_2} \sqrt{\frac{2j_3+1}{2j_1+1}} C_{-m_2 m_3 m_1}^{j_2 j_3 j_1}, \\ C_{m_1 m_2 m_3}^{j_1 j_2 j_3} &= (-1)^{j_1+j_2-j_3} C_{-m_1 -m_2 -m_3}^{j_1 j_2 j_3}. \end{aligned} \quad (55)$$

We finally find

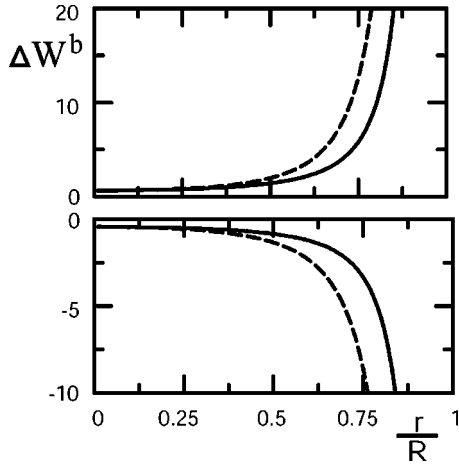


FIG. 7. Image interaction ΔW^b from Eq. (57) between the surface and a cellular force dipole embedded in an elastic sphere of radius R with $\nu=1/3$, plotted in units of P^2/ER^3 as a function of distance r/R to the sphere surface and rescaled by $15/8$. Curves above and below the r axis correspond to free and clamped boundary conditions, respectively. Solid and dashed lines correspond to orientations $\theta=\pi/2$ and $\theta=0$ with respect to the surface normal. As for the half space, optimal cell orientation yields $\theta=0$ (clamped) and $\theta=\pi/2$ (free), respectively.

$$u_{\alpha}^{\beta}(\vec{r}, \vec{r}') = \sum_{lm} R^l \frac{a_{lm}}{1+\Lambda} X^{*\alpha\beta} \left(\frac{r}{R}, \Omega \right) - (2l+3) r^l A^{*\alpha\beta}(\Omega) \times \left(\frac{b_{l+2m}}{2} C_{m-\alpha}^{l+1} C_{m-\alpha}^{l+2} + c_{l+1m} C_{m-\alpha}^{l+1} C_{m-\alpha}^{l+1} \right). \quad (56)$$

Note that the m sums over b_{lm} and c_{lm} run in the intervals $[-l-2, l+2]$ and $[-l-1, l+1]$, respectively. The boundary induced change in stiffness sensed by a force dipole in an elastic sphere is then found by inserting the appropriate expansion coefficients a_{lm} , etc. given in Eqs. (50) and (51) and contracting u_{α}^{β} with $P^{\alpha}_{\beta} = P'^{\alpha}_{\beta}$. We may rewrite ΔW^b to indicate the important scaling laws of the interaction of the dipole with the sphere surface by

$$\Delta W^b = \frac{P^2}{ER^3} f_{\nu} \left(\frac{r}{R}, \theta \right), \quad (57)$$

where r is the distance to the sphere center and θ is the dipole orientation with respect to the surface normal. The function f_{ν} contains the sum over all angular momenta and does not vary qualitatively as ν (or, equivalently, Λ) is varied. With regard to cell orientation, we find the same results as for the elastic half space: cells will orient parallel (perpendicular) to a free (clamped) surface, respectively. As shown in Fig. 7, we also find a similar result for the effect of distance to the surface; for free (clamped) boundary conditions, a small (large) distance to the sphere center is more favorable, since the surface favors (disfavors) mechanical activity. The new aspect here is the role of the sphere radius R . Since $|\Delta W|$ increases when R decreases, one can effectively rigidify (soften) a material with a clamped (free) surface by

reducing system size. For the interaction of a physical dipole with the surface embedded in an elastic sphere, we once more obtain the opposite results. Dipoles are attracted (repelled) and orient towards (away from) a free (clamped) surface.

So far we have considered the interaction of a force dipole with the boundary. One may extend our model of cell-cell interactions to cells embedded in finite geometries and study how their boundaries alter the interaction between cells. In an elastic sphere containing many cells, we can separate the contributions to the effective stiffness into a contribution from the boundary induced field, i.e., a cell-surface interaction as discussed above, and a contribution from the elastic fields of other cells embedded in the sphere, i.e., a cell-cell interaction term. This contribution is modified with respect to the interaction term in infinite medium, Eq. (27), by a boundary mediated interaction term. The indirect interaction term is given by contracting the dipole tensor of the first dipole with the image strain caused by the second dipole. The most important result here is that the image term varies on the macroscopic scale R . For physical dipoles, elastic interactions in finite sized geometries have been studied extensively, in particular for *isotropic* dipoles, which do not interact in infinite medium and where the interaction between dipoles is mediated solely via the boundary [23]. By setting $P_{\alpha}^{\beta} = \delta_{\alpha\beta}$ our results specialize to the interaction of isotropic dipoles in an elastic sphere

$$\Delta W^b(\vec{r}, \vec{r}') = -V^b(\vec{r}, \vec{r}') = \sum M_l r^l r'^l Y_{lm}^*(\Omega) Y_{lm}(\Omega') \quad (58)$$

with

$$M_l^f = \frac{PP'}{cR^3} \frac{2(2l+3)(l+1)(l+2)}{2(l^2+l+1)+\Lambda(2l^2+4l+3)}, \quad (59)$$

$$M_l^c = -\frac{PP'}{cR^3} \frac{2l+3}{(l+1)(1+(\Lambda+3)l)} \quad (60)$$

for free and clamped boundaries, respectively. These results can be shown to be identical with the ones for isotropic dipoles previously reported in Ref. [23]. Note that the interaction of physical isotropic defects is always attractive (repulsive) for isotropic dipoles in a free (clamped) sphere. Due to the macroscopic interaction range of isotropic physical dipoles the indirect interactions lead to structure formation on the macroscopic scale (*macroscopic modes*), e.g., in hydrogen-metal alloys [23]. For anisotropic dipoles the image interaction introduces corrections to the direct interaction term, which vary on the macroscopic scale. In Fig. 8 we plot the interaction of two anisotropic dipoles in infinite medium and the modified interactions in clamped and free spheres, respectively. For example, the image correction in a free sphere for two parallel z dipoles (one placed at the sphere center) along the x axis reads

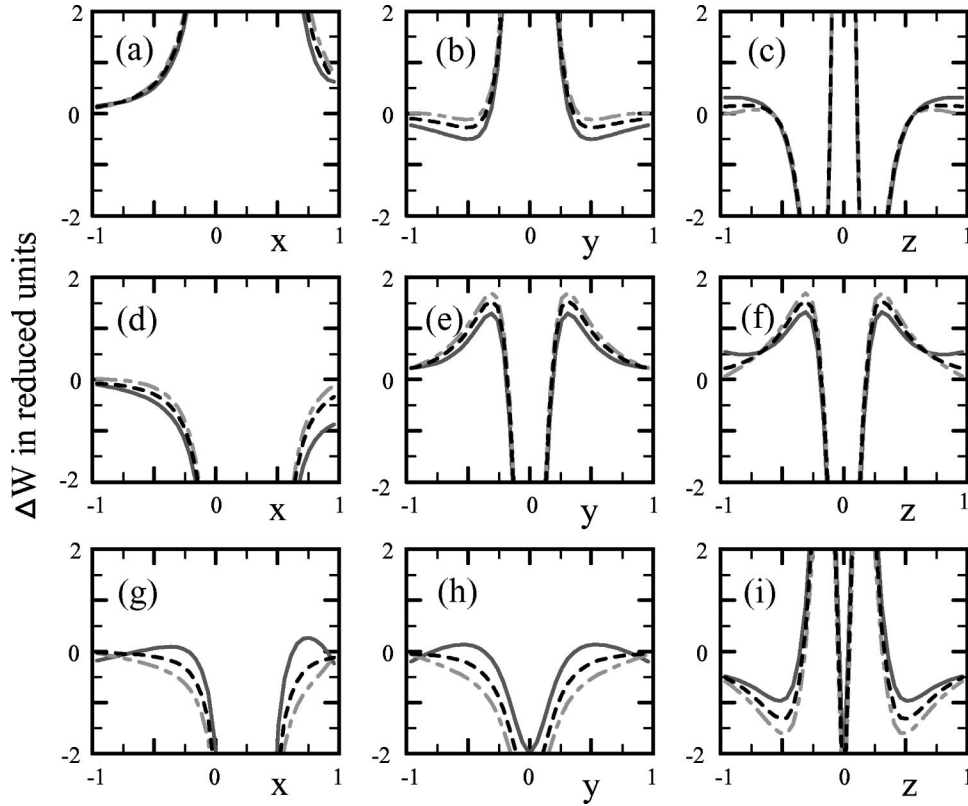


FIG. 8. Cellular dipole-dipole interactions $\Delta W = \Delta W^\infty + \Delta W^b$ in an elastic sphere ($\Lambda=2$) in units of PP'/cR^3 for clamped (dashed gray) and free (full gray) boundary conditions. A z dipole is fixed at $\vec{r} = (R/4, 0, 0)$. A x dipole (a,b,c), y dipole (d,e,f), and z dipole (g,h,i) is moved along the coordinate axes. The boundary condition introduces corrections to the interaction in infinite medium (black line) that vary on the macroscopic scale. The boundary term dominates close to the surface and in some cases introduces new maxima or minima in the interaction landscape.

$$\Delta W^b(x) = \frac{PP' \left[(112 + 352\Lambda + 370\Lambda^2 + 135\Lambda^3) - 12(7 + 4\Lambda)(2 + 5\Lambda + 3\Lambda^3) \left(\frac{x}{R} \right)^2 \right]}{4(2 + 3\Lambda)(14 + 19\Lambda)\pi c R^3}. \quad (61)$$

For $\Lambda \rightarrow \infty$ ($\nu=1/2$), this becomes

$$\Delta W^b(x) = \frac{PP'}{76\pi\mu R^3} \left[45 - 48 \left(\frac{x}{R} \right)^2 \right]. \quad (62)$$

For a clamped sphere, we find

$$\Delta W^b(x) = \frac{PP' \left[-(686 + 280\Lambda + 24\Lambda^2) + 45(1 + \Lambda)(7 + 4\Lambda) \left(\frac{x}{R} \right)^2 \right]}{120(7 + 2\Lambda)\pi c R^3}, \quad (63)$$

which for $\nu=1/2$ becomes

$$\Delta W_c^b(x) = \frac{PP'}{20\pi\mu R^3} \left[-2 + 15 \left(\frac{x}{R} \right)^2 \right]. \quad (64)$$

Again we find that clamped and free surface result in opposite effects. On the microscopic scale (i.e., for small cell-cell

distances), the direct interaction dominates. For macroscopic cell separations, the boundary term introduces significant contributions that dominate over the direct term close to the surface. For some cases, the boundary can induce new maxima or minima in the dipole-dipole interaction landscape. Note that for a full treatment, the dipole-surface interactions have to be included. In conclusion, in contrast to isotropic dipoles, structure formation of anisotropic dipoles

is dominated by effects on cellular and elastic scales, which result from direct interactions. Since they compete with boundary induced effects on a macroscopic scale, in general we expect hierarchical structures.

F. Summary example section

In the second part of this paper, we applied the general formalism from the first part to different situations of interest. In general, we found that physical and cellular force dipoles interact in opposite ways with each other, external strain field or sample boundaries, because $V_i = -W$. For example, physical anisotropic force dipoles on top of thick elastic films or in infinite elastic material locally prefer the T configuration (for Poisson ratio $\nu=1/2$), while cellular anisotropic force dipoles align in strings (independent of the value for ν). The predicted structure formation for physical force dipoles and active cells is similar to the ones of electric quadrupoles and dipoles, respectively. We also found that in general, free and clamped boundaries will have opposite effects. For example, cellular anisotropic force dipoles are repelled and attracted by free and clamped boundaries, respectively. In the vicinity of these boundaries, they will align in parallel and perpendicular, respectively. In general, all the interaction laws derived here show the universal scaling $W \sim (P^2/El^3)f_\nu(\theta_i)$, where f is a nontrivial function of Poisson ratio ν and the different angles θ_i , which has to be calculated for each situation of interest. Except for the case of external strain, the cellular force pattern interacts with itself (case of boundaries) or with another cellular force pattern (case of elastic interaction of cells), therefore $W \sim P^2$. The scaling $W \sim 1/l^3$ is typically for force dipoles. Here the length l can either be distance (e.g., between cell and boundary or between two cells) or sample size (in the elastic sphere). Finally, $W \sim 1/E$. Although W decreases with increasing Young modulus E , that is, elastic effects become smaller, at the same time mechanical activity of cells usually increases. For this reason, we expect that there exists a range of optimal values for E for which the elastic effects in cell adhesion described here should be most pronounced (possibly around $E = \text{kPa}$, the physiological order of magnitude for cell and tissue stiffness).

Although our modeling focuses on the role of strain and stress in the extracellular environment, we also need a model for the typical force pattern of mechanically active cells. Since the minimal system for contractile activity of adherent cells is one stress fiber connecting two focal adhesions, we

introduced the concept of force dipoles into the physics of cells [29]. From a technical point of view, this allowed us to make contact to a large body of results on physical force dipoles in deformable media. Our theory reproduces known results for physical force dipoles, in particular, the elastic image interaction of isotropic force dipoles in a free elastic sphere [23]. The corresponding calculation for anisotropic dipoles has been done before by Hirsekorn and Siems [36], but only for the free surface. Here we extended this calculation to the clamped case. Moreover, in order to predict single cell effects, we also calculated the interaction between dipole and surface for both types of boundary condition. In contrast to the elastic sphere for the elastic half space an image system for the effect of force monopoles is known [35]. Here we used the solution given by Walpole [39] and adapted it for the case of force dipoles.

As reported earlier, our predictions for cell organization in soft media are in excellent agreement with experimental observations [31]. Our theory not only contributes to a better understanding of physiological processes involving mechanical activity of cells (including tissue maintenance, wound healing, angiogenesis, development, and metastasis), in the future it also might be used to predict cell behavior in artificial tissues, close to implants and on compliant biosensors. Moreover, the orientation response of regulated cells as described here might be used to distinguish between healthy and diseased conditions. It is important to note that the main success of our model results from the fact that we focus on the role of stress and strain in the environment, which allows us to use the concepts of linear elasticity theory and to make minimal assumptions about cellular regulation. In the future, our theory might be complemented by models for cell morphology and the dynamics of focal adhesions. Moreover, until now we did not address in detail the issue of structure formation within large communities of cells, although this might be of much importance for development, when large groups of mechanical active cells are known to move in concert.

ACKNOWLEDGMENTS

I.B.B. thanks Thomas Pfeifer for helpful discussions. S.A.S. acknowledges support by the Schmidt Minerva Center, the Israel Science Foundation and the U.S. Israel Binational Science Foundation. I.B.B. and U.S.S. are supported by the German Science Foundation through the Emmy Noether Program.

-
- [1] A.K. Harris, P. Wild, and D. Stopak, *Science* **208**, 177 (1980).
 - [2] A.K. Harris, D. Stopak, and P. Wild, *Nature (London)* **290**, 249 (1981).
 - [3] M. Dembo, T. Oliver, A. Ishihara, and K. Jacobson, *Biophys. J.* **70**, 2008 (1996).
 - [4] M. Dembo and Y.-L. Wang, *Biophys. J.* **76**, 2307 (1999).
 - [5] N.Q. Balaban *et al.*, *Nat. Cell Biol.* **3**, 466 (2001).
 - [6] U.S. Schwarz, N.Q. Balaban, D. Rivelino, A. Bershadsky, B. Geiger, and S.A. Safran, *Biophys. J.* **83**, 1380 (2002).
 - [7] J.L. Tan, J. Tien, D.M. Pirone, D.S. Gray, K. Bhadriraju, and C.S. Chen, *Proc. Natl. Acad. Sci. U.S.A.* **100**, 1484 (2003).
 - [8] J. Howard, *Mechanics of Motor Proteins and the Cytoskeleton* (Sinauer Associates, Sunderland, MA, 2001).
 - [9] G.F. Oster, J.D. Murray, and A.K. Harris, *J. Embryol. Exp. Morphol.* **78**, 83 (1983).
 - [10] V.H. Barocas and R.T. Tranquillo, *J. Biomech. Eng.* **119**, 137 (1997).
 - [11] R.J. Pelham and Y.-L. Wang, *Proc. Natl. Acad. Sci. U.S.A.* **94**,

- 13 661 (1997).
- [12] C.-M. Lo, H.-B. Wang, M. Dembo, and Y.-L. Wang, *Biophys. J.* **79**, 144 (2000).
- [13] J.Y. Wong, A. Velasco, P. Rajagopalan, and Q. Pham, *Langmuir* **19**, 1908 (2003).
- [14] B. Geiger and A. Bershadsky, *Cell* **110**, 139 (2002).
- [15] N. Wang, J.P. Butler, and D.E. Ingber, *Science* **260**, 1124 (1993).
- [16] D. Choquet, D.F. Felsenfeld, and M.P. Sheetz, *Cell* **88**, 39 (1997).
- [17] D. Riveline, E. Zamir, N.Q. Balaban, U.S. Schwarz, B. Geiger, Z. Kam, and A.D. Bershadsky, *J. Cell Biol.* **153**, 1175 (2001).
- [18] M.E. Chicurel, C.S. Chen, and D.E. Ingber, *Curr. Opin. Cell Biol.* **10**, 232 (1998).
- [19] C.G. Galbraith and M. Sheetz, *Curr. Opin. Cell Biol.* **10**, 566 (1998).
- [20] S. Huang and D.E. Ingber, *Nat. Cell Biol.* **1**, E131 (1999).
- [21] B. Geiger, A. Bershadsky, R. Pankov, and K. Yamada, *Nat. Rev. Mol. Cell Biol.* **2**, 793 (2001).
- [22] R. Siems, *Phys. Status Solidi* **30**, 645 (1968).
- [23] H. Wagner and H. Horner, *Adv. Phys.* **23**, 587 (1974).
- [24] K.H. Lau and W. Kohn, *Surf. Sci.* **65**, 607 (1977).
- [25] S.A. Safran and D.R. Hamann, *Phys. Rev. Lett.* **42**, 1410 (1979).
- [26] S. Ramaswamy, J. Toner, and J. Prost, *Phys. Rev. Lett.* **84**, 3494 (2000).
- [27] P. Lenz, J.-F. Joanny, F. Jülicher, and J. Prost, *Phys. Rev. Lett.* **91**, 108104 (2003).
- [28] R.A. Simha and S. Ramaswamy, *Phys. Rev. Lett.* **89**, 058101 (2002).
- [29] U.S. Schwarz and S.A. Safran, *Phys. Rev. Lett.* **88**, 048102 (2002).
- [30] J.P. Butler, I.M. Tolic-Norrelykke, B. Fabry, and J.J. Fredberg, *Am. J. Physiol. Cell Physiol.* **282**, C595 (2002).
- [31] I.B. Bischofs and U.S. Schwarz, *Proc. Natl. Acad. Sci. U.S.A.* **100**, 9274 (2003).
- [32] F. Grinnell, *Trends Cell Biol.* **10**, 362 (2000).
- [33] A.E.H. Love, *A Treatise on the Mathematical Theory of Elasticity* (Dover, New York, 1944).
- [34] L.D. Landau and E.M. Lifshitz, *Theory of Elasticity*, 2nd ed., Course of Theoretical Physics, Vol. 7 (Pergamon Press, Oxford, 1970).
- [35] R.D. Mindlin, *Physics* **7**, 195 (1936).
- [36] R.-P. Hirsekorn and R. Siems, *Z. Phys. B: Condens. Matter* **40**, 311 (1981).
- [37] T. Tlusty and S.A. Safran, *Science* **290**, 1328 (2000).
- [38] N. Phan-Thien, *J. Elast.* **13**, 231 (1983).
- [39] L.J. Walpole, *Int. J. Eng. Sci.* **34**, 629 (1996).
- [40] A.R. Edmonds, *Angular Momentum in Quantum Mechanics*, 3rd ed. (Princeton University Press, Princeton, N.J., 1974).